Designing Efficient Observing Networks for ENSO Prediction

REBECCA E. MORSS

National Center for Atmospheric Research, Boulder, Colorado*

DAVID S. BATTISTI

Joint Institute for the Study of the Atmosphere and Ocean, University of Washington, Seattle, Washington

(Manuscript received 16 June 2003, in final form 10 February 2004)

ABSTRACT

The Tropical Atmosphere Ocean (TAO) array of moored buoys in the tropical Pacific Ocean is a major source of data for understanding and predicting El Niño–Southern Oscillation (ENSO). Despite the importance of the TAO array, limited work has been performed where observations are most important for predicting ENSO effectively. To address this issue, this study performs a series of observing system simulation experiments (OSSEs) with a linearized intermediate coupled ENSO model, stochastically forced. ENSO forecasts are simulated for a variety of observing network configurations, and forecast skill averaged over many simulated ENSO events is compared.

The first part of this study examined the relative importance of sea surface temperature (SST) and subsurface ocean observations, requirements for spacing and meridional extent of observations, and important regions for observations in this system. Using these results as a starting point, this paper develops efficient observing networks for forecasting ENSO in this system, where efficient is defined as providing reasonably skillful forecasts for relatively few observations. First, efficient networks that provide SST and thermocline depth data at the same locations are developed and discussed. Second, efficient networks of only thermocline depth observations are addressed, assuming that many SST observations are available from another source (e.g., satellites). The dependence of the OSSE results on the duration of the simulated data record is also explored. The results suggest that several decades of data may be sufficient for evaluating the effects of observing networks on ENSO forecast skill, despite being insufficient for evaluating the long-term potential predictability of ENSO.

1. Introduction

The last decade has seen major advances in understanding, modeling, and predicting El Niño–Southern Oscillation (ENSO; see, e.g., review papers by Wallace et al. 1998 and McPhaden et al. 1998). Despite these advances, our ability to forecast the evolution of the ENSO system is currently far from perfect, particularly at lead times of several seasons or more (e.g., Latif et al. 1998). Errors in ENSO forecasts can occur for several reasons, including 1) errors in the models used to generate forecasts, 2) errors in the initial conditions used to initiate forecasts, and 3) characteristics of the coupled tropical ocean–atmosphere system that limit potential predictability, such as error growth and atmospheric noise. Although each of these has been investigated in a number of studies, they interact in ways that complicate identifying the causes of current limitations in ENSO forecast skill. For example, because the models used to predict ENSO are imperfect, when studying ENSO prediction with real data it can be difficult to diagnose whether forecast errors are due primarily to model errors, data–model incompatibility, inadequate data assimilation, or insufficient observations of the initial state.

Such difficulties are exacerbated by the limited duration of the data record available for studies of ENSO prediction. For example, the Tropical Atmosphere Ocean (TAO) array of moored buoys in the tropical Pacific, a major source of observations for understanding and predicting ENSO, was only completed in the early 1990s (Hayes et al. 1991). Other major sources of tropical Pacific data, such as ships, tide gauges, and satellites, also have limited spatial or temporal coverage. The limited data record may be problematic because the potential predictability of ENSO may vary within the available data record (e.g., Balmaseda et al. 1995; Chen et al. 1995; Ji et al. 1996; Fischer et al. 1997; Kirtman and Schopf 1998), and forecast errors for different ENSO events may have different causes (e.g., Chen et

* The National Center for Atmospheric Research is sponsored by the National Science Foundation.

Corresponding author address: Dr. Rebecca E. Morss, National Center for Atmospheric Research, P.O. Box 3000, Boulder, CO 80307. E-mail: morss@ucar.edu

al. 1995; Ji et al. 1996; Chen et al. 1998; Federov and Philander 2000; Perigaud et al. 2000). Consequently, current understanding of how well the existing tropical ocean–atmosphere observing system satisfies data requirements for ENSO prediction is limited (e.g., Latif et al. 1998).

As a complement to studies of ENSO-observing requirements with real data, this study investigates where observations are important for skillful ENSO prediction by performing observing system simulation experiments (OSSEs) with an intermediate coupled dynamical ENSO model and a three-dimensional variational data assimilation system (3DVAR). The OSSEs generate synthetic observations by sampling from a model run that simulates the evolution of the true ENSO system. The model used (Thompson and Battisti 2000) is a linearized variant of the Zebiak–Cane (1987) ENSO model, with stochastic forcing to simulate atmospheric noise. Although not a general requirement for OSSEs, this initial study uses the same dynamical model to evolve the simulated real and forecast states. The OSSEs implemented here are therefore similar to standard ''identical twin'' experiments.

Because the experiments simulate ENSO events and observations, they are not limited by the available data record. Results can therefore be compared for a variety of hypothetical configurations of observations in a large number of cases. In addition, by using the same dynamical model to simulate forecasts and the real system, these experiments eliminate two of the factors that complicate interpreting results from studies with real data: errors in model dynamics and model–initial condition incompatibility. However, OSSEs also have limitations. Most importantly, the experiments are only relevant to the real world to the extent that the simulated ENSO system adequately represents real ENSO dynamics. The results presented here cannot therefore be applied directly to the real ENSO-observing system. Nevertheless, the experiments do contribute to our understanding of ENSO-observing requirements, and in doing so suggest considerations for future studies of ENSO-observing network design.

The first part of this study, Morss and Battisti (2004; hereafter MB1), demonstrated the basic forecast behavior of the system using results from OSSEs with persistence forecasts, perfect initial conditions, and many sea surface temperature (SST) and/or thermocline depth observations. MB1 then explored how ENSO forecast skill in this system is affected by varying the spacing and locations of observations. In doing so, they identified general regions where good information about the initial conditions contributes most to ENSO forecast skill: 1) south of the equator, east of approximately 130°W and 2) the western equatorial Pacific. They also noted that these regions coincide with those where the leading singular vector and adjoint-derived sensitivities for the ENSO model used have the largest amplitudes.

This paper builds on the results in MB1 by developing observing networks that are efficient for ENSO prediction in this system, where efficient is defined as providing reasonably skillful forecasts for a relatively small number of observations. Given the idealized experimental setup and idealized observing platforms tested, the efficient networks presented are not meant to identify specific locations for TAO moorings; rather, they indicate general regions where good information about initial conditions may be important, from observing platforms of any type. Because a major difference between this study and many other studies of ENSO prediction is the number of ENSO events examined, the dependence of the OSSE results on the duration of the simulated data record is also explored.

Section 2 reviews the experimental design, including the ENSO prediction model, the simulated observations, the data assimilation system, and the setup of the OSSEs; a more detailed description can be found in MB1. Section 3 develops and discusses two types of efficient observing networks: networks when SST and thermocline depth data are taken at the same locations and networks of thermocline depth observations when many SST observations are available from another source (e.g., satellites). Section 4 explores the effects of averaging results over simulated data records of different durations. In section 5, the study's results are summarized and discussed.

2. Experimental design

This section reviews major aspects of the experimental design. A complete description of the numerical model physics and behavior can be found in Thompson (1998) and Thompson and Battisti (2000, 2001); a summary is provided in MB1. A complete description of the simulated observations, data assimilation system, and setup of the OSSEs can be found in MB1.

a. Numerical prediction model

The prediction model used is the stochastically forced, intermediate coupled T80 ENSO model described in Thompson and Battisti (2000, 2001). The model is a linearized variant of the Zebiak–Cane (1987) ENSO model, consisting of a 1½-layer dynamic ocean model in a rectangular Pacific basin coupled to a Gill (1980) two-layer model of the tropical atmosphere. The development of the T80 model, the selection of the model parameters, and the stochastic forcing are summarized in MB1; with this configuration, the model reproduces the observed level of interannual variability in Niño-3 SST and other ENSO indices, and its leading mode is similar to the observed ENSO mode (Thompson and Battisti 2000, 2001). The T80 model is moderately damped, so that all ENSO events are the result of transient growth initiated by the stochastic forcing (which simulates atmospheric noise).

The prognostic model variables are ocean dynamics,

which includes thermocline depth and ocean surface currents, and SST. Atmospheric surface winds are obtained diagnostically from the SST. In longitude, the model domain extends from 123°E to 81°W and is discretized at 15 equally spaced grid points. In latitude, the model is discretized in terms of Hermite polynomials for SST, and Kelvin and Rossby waves for the ocean dynamics. For SST, eight Hermite polynomials are retained; for ocean dynamics, the Kelvin wave and eight Rossby waves are retained.

The OSSE methodology, described in section 2d, uses the numerical model to generate synthetic ENSO events. Consequently, the study's results are only applicable to the real world to the extent that the model can be considered representative of the real ENSO system. The model used here is closely related to the Zebiak–Cane (1987) model (Chen et al. 1997; Thompson 1998), which is well established, has been used in numerous studies, and has predictive skill similar to that of other ENSO models (Latif et al. 1998). Thus, the model simulates ENSO dynamics sufficiently well to be useful for an OSSE study. Nevertheless, only a limited set of dynamics and types of ENSO events are included in the model, and the results should be interpreted with this in mind.

b. Simulated observations

Two types of observations are simulated: SST and thermocline depth. Each is observed once per month, simulating monthly averaged data. Assimilating SST data is similar to inserting surface wind information; assimilating thermocline depth is similar to assimilating upper-ocean heat content or sea level information.

All observations are assumed to have independent errors. The standard deviations of the errors in the SST and thermocline depth observations are set to 0.2°C and 2 m, respectively. Although more sophisticated observation errors could easily be simulated, we chose to simulate relatively simple ones to facilitate interpreting the effects of modifying the observing network. Given the simple form of the simulated observations, the results can be interpreted as identifying general regions in which SST and/or upper-ocean heat content observations are important for skillful ENSO prediction in this system.

c. Data assimilation system

The simulated observations are incorporated into the model state using a 3DVAR data assimilation system, similar to the scheme described in Derber and Rosati (1989) and currently used operationally at the National Centers for Environmental Prediction (NCEP; Ji et al. 1995). Observations are assimilated once per month, with no temporal smoothing.

The background error covariance matrix used is time invariant; it assumes that SST and ocean dynamics errors are uncorrelated with each other and that errors in different latitudinal projections are uncorrelated. The longitudinal correlation length of background errors is set to 1300 km for both SST and ocean dynamics. The scale of the background errors is selected so that for a single observation near the equator, the observation and the background field are weighted approximately equally. Analysis increments for a single SST observation and a single thermocline depth observation are shown in MB1.

As discussed in MB1, the numerical model has sufficiently few degrees of freedom that a more sophisticated data assimilation system could readily be implemented. We chose to use 3DVAR and simple error statistics, however, to facilitate interpreting the effects of modifying the observing network. Due to the simplicity of the data assimilation system, the effects of adding or removing observations in a variable and region can, in general, be interpreted in terms of how important good information about the initial conditions in that variable and region is for producing skillful ENSO forecasts.

d. OSSEs

The OSSEs contain two parallel runs of the ENSO model: a ''true'' run that simulates the evolution of the true ENSO system, and an ''analysis/forecast'' run that simulates a sequence of analyses and forecasts. Once per month, observations are created by sampling from the true run and adding random errors. These observations are then assimilated into the analysis/forecast run using 3DVAR. The resulting analysis is used to simulate ENSO forecasts out to 24 months, with the 1-month forecast becoming the background (first guess) field for the assimilation at the next observation time. The true run, the analysis/forecast run, and the 24-month forecasts are integrated forward using the same dynamical model, with different realizations of the stochastic forcing. The experiments performed here are thus similar to standard identical twin experiments, but simulate model error through the stochastic forcing.

Each OSSE has the same sequence of ENSO states in the true run, so that the same time series of ENSO events is being predicted. All analyses and forecasts are evaluated with respect to the corresponding state in the true run. Four error norms were implemented: anomaly correlation (AC) of the Niño-3 SST index, and rmse in SST in the Niño-3 region (5°S–5°N, 150°–90°W), the Niño-3.4 region (5°N–5°S, 170°–120°W), and the equatorial region (10°S–10°N). Most of the results shown are for skill statistics accumulated over 1000 years of events; results averaged over shorter periods of time are discussed in section 4. Prior to gathering skill statistics, each OSSE is run for a 20-yr spinup period to equilibrate the analysis/forecast run to the observing network.

OSSEs have three major advantages compared to experiments with real data: 1) complete information is available about the state of the system being predicted,

TABLE 1. Description of the reference experiments used as a baseline for interpreting the results.

Experiment	Description
PerfectIC	Standard OSSE, except that at each assimilation time, the initial model state is set to the true state (OSSE with perfect initial conditions).
FullTh	Standard OSSE, with 375 simulated SST and thermocline depth observations at the locations shown in Fig. 1.
FullT	Standard OSSE, with SST observations at the same 375 locations as in FullTh (no thermocline depth observations).

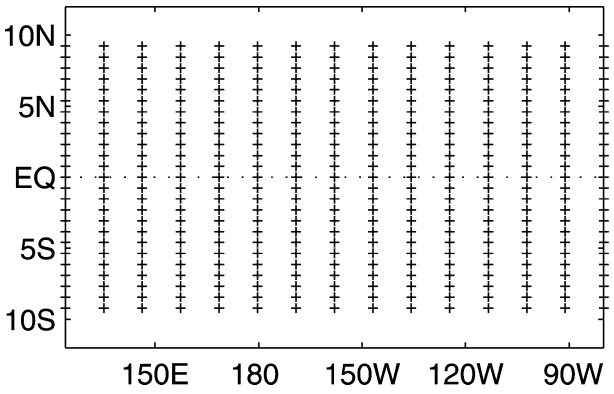

FIG. 1. Locations of the 375 observations in the FullTh network: at 15 longitudes, spaced by 11°, and at 25 latitudes, spaced by 0.77°, from 9.2°S to 9.2°N.

2) any observing network that can be simulated can be tested, and 3) the number of cases that can be investigated is limited only by computational resources. However, OSSEs also have a major disadvantage: the results are only applicable to the real world to the extent that the simulated system represents the real system. There are two major aspects of these experiments that may limit their applicability to the real world: the simulated observations are idealized, and the model used to generate the true run is a simplified representation of the true coupled atmosphere–ocean system.

e. Reference experiments

Results from three reference experiments, described in Table 1, are used in subsequent sections as a baseline for interpreting results. In the PerfectIC experiment, forecasts are generated from perfect initial conditions. In the FullTh experiment, simulated SST and thermocline depth observations are taken and assimilated at the 375 locations depicted in Fig. 1. The FullTh experiment generates nearly perfect initial conditions, and FullTh forecasts are nearly as accurate as PerfectIC forecasts. Thus, both the PerfectIC and FullTh results are measures of the maximum forecast skill attainable in this system by improving the initial conditions. In the FullT experiment, observations are taken at the same 375 locations as in the FullTh experiment, but only of SST. Results from all three experiments are discussed in greater detail in MB1.

3. Efficient observing networks

This section presents several observing networks that are efficient for predicting ENSO in this system, where efficient is defined as providing reasonably skillful forecasts for a relatively small number of observations. Section 3a discusses networks that observe SST and thermocline depth at the same locations; section 3b discusses networks of only thermocline depth observations, assuming that many SST observations are available from another source. As in MB1, all observing locations remain fixed throughout each experiment, and results are averaged over 1000-yr OSSEs.

To design the efficient observing networks, we compared the average skill of forecasts produced by various configurations of observations at a range of lead times. Skill was compared in each of the four norms implemented (Niño-3 SST AC, and rmse in Niño-3, Niño-3.4, and equatorial Pacific SST). In situations where the network that produced more skillful forecasts depended on the forecast norm and/or lead time, the greatest weight was given to 3–9-month forecasts; at these lead times, comparisons are generally similar using different norms. Based on results from MB1, none of the networks tested have observations poleward of 9.2°N/S.

Given the idealized experimental setup—particularly the simplified dynamics in the ENSO model—aspects of the results from this study may not apply to the real ENSO system. In addition, the number and placement of observations in an efficient observing network depends on factors not addressed in this study, such as the data assimilation system, the forecast model, and the characteristics of the available observing platforms. Thus, the efficient observing networks depicted here are not presented as designs for the real ENSO-observing network. Rather, the results are presented to demonstrate the general regions in which observations are important in this system, and to identify general features of ENSO-observing networks that merit further investigation.

a. Efficient networks that observe SST and thermocline depth at the same locations

As discussed in MB1 and section 2e, results from the PerfectIC experiment (solid line in Fig. 2) represent the maximum average forecast skill attainable by improving the initial conditions. Forecasts from the FullTh network, which contains 375 SST and thermocline observations at the locations depicted in Fig. 1, are nearly as skillful as PerfectIC forecasts (cf. the solid and dashed lines in Fig. 2). To illustrate the design of the efficient SST-and thermocline-observing networks discussed in this section, we therefore start with the FullTh network

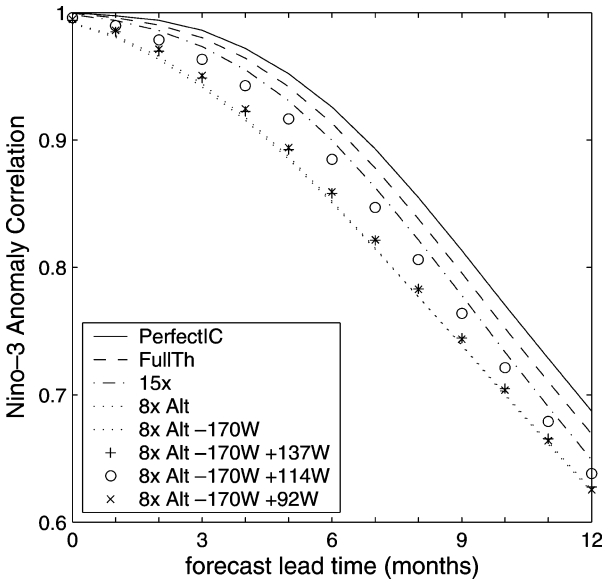

FIG. 2. The AC of the Niño-3 SST index for initial conditions (forecast lead time = 0 months) and 1–12 month forecasts for various observing networks. Results are averaged over a 1000-yr OSSE. The solid line depicts results from the PerfectIC experiment, and the dashed line depicts results for the FullTh experiment, both described in Table 1; each is an estimate of the maximum attainable forecast skill. All of the remaining observing networks tested contain several north–south transects with observations at 7 latitudes: 9.2°S, 6.9°S, 4.6°S, 2.3°S, 0°, 2.3°N, and 4.6°N. The 15x network has north–south transects at each longitudinal grid point (15 spaced by 11°; 105 observing locations). The 8x Alt network has transects at every other longitudinal grid point (8 spaced by 22°; 56 observing locations). The 8x Alt−170W network has transects at the same locations as the 8x Alt network, but no transect at 170°W (49 observing locations). The 8x Alt−170W+137W, 8x Alt−170W+114W, and 8x Alt−170W+92W networks have transects at the same locations as the 8x Alt network, but with the transect at 170°W moved to 137°, 114°, and 92°W, respectively (56 observing locations each). Note that the 8x Alt−170W+114W network is the same as the EFF56 network. depicted in Fig. 3.

and then examine the effects of removing various observations.

The FullTh network can be thought of as 15 north–south transects, each of which contains observations at the same 25 latitudes. First, we vary the meridional locations of the observations within the north–south transects. Based on the results from varying the meridional spacing of observations in MB1, the meridional spacing is increased from 0.77° to 2.3°. In addition, since MB1 found that observations north of approximately 4.6°N contribute little to forecast skill, observations north of 4.6°N are removed. The resulting network has 105 observations, at 7 latitudes from 9.2°S to 4.6°N, at each of the 15 longitudinal grid points. As shown by the 15x results in Fig. 2, this network produces forecasts that are only slightly (approximately 1%–3%) less skillful than FullTh forecasts, even though it observes at less than 30% of the locations in the FullTh network.

Keeping observations at 7 latitudes from 9.2°S to 4.6°N, we then modify the longitudinal locations of the

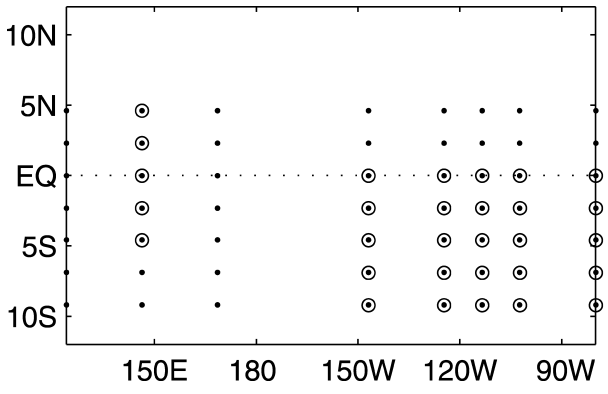

FIG. 3. Locations of the 56 SST and thermocline depth observations in the EFF56 network (small dots) and the 30 SST and thermocline depth observations in the EFF30 network (circles), described in Table 2.

observations, that is, the longitudes of the north–south transects. First, based on the results from varying the longitudinal spacing of observations in MB1, the longitudinal spacing is increased from 11° to 22° (every other longitudinal grid point). As shown by the 8x Alt results in Fig. 2, this degrades forecasts somewhat, but not dramatically. Next, based on the result from MB1 that observations are least important in the central equatorial Pacific and most important in the eastern equatorial Pacific, we test moving a north–south transect from the central Pacific into the eastern Pacific. As shown by the 8x Alt−170W results in Fig. 2, removing all of the observations at 170°W, near the center of the domain, does not noticeably degrade analyses or forecasts. When the observations removed from 170°W are placed at 137° or 92°W (both longitudinal grid points unobserved in the 8x Alt network), forecast skill increases by only a very small amount. When the observations are moved from 170° to 114°W, on the other hand, forecast skill increases significantly—in fact, as illustrated in Fig. 2, forecasts from the 8x Alt−170W+114W network are nearly as skillful as those when observations are taken at all 15 longitudes. Consequently, this network becomes our first efficient observing network. Called EFF56, it contains 56 SST and thermocline depth observations at the locations indicated by the small dots in Fig. 3.

Results from a number of other experiments indicated that, of the observed regions in EFF56, observations are least important at the western boundary, at 168°E, north of the equator in the central-eastern Pacific, and south of 5°S in the western Pacific. Using this information, we removed nearly half of the observations in EFF56 to design a second efficient observing network. Called EFF30, this network contains 30 SST and thermocline depth observations at the locations indicated by the circles in Fig. 3.

Figure 4 shows the average skill of analyses and forecasts from EFF56, EFF30, and the EQSP56, EFF56x2. and EFF56y2 networks described in Table 2. Results

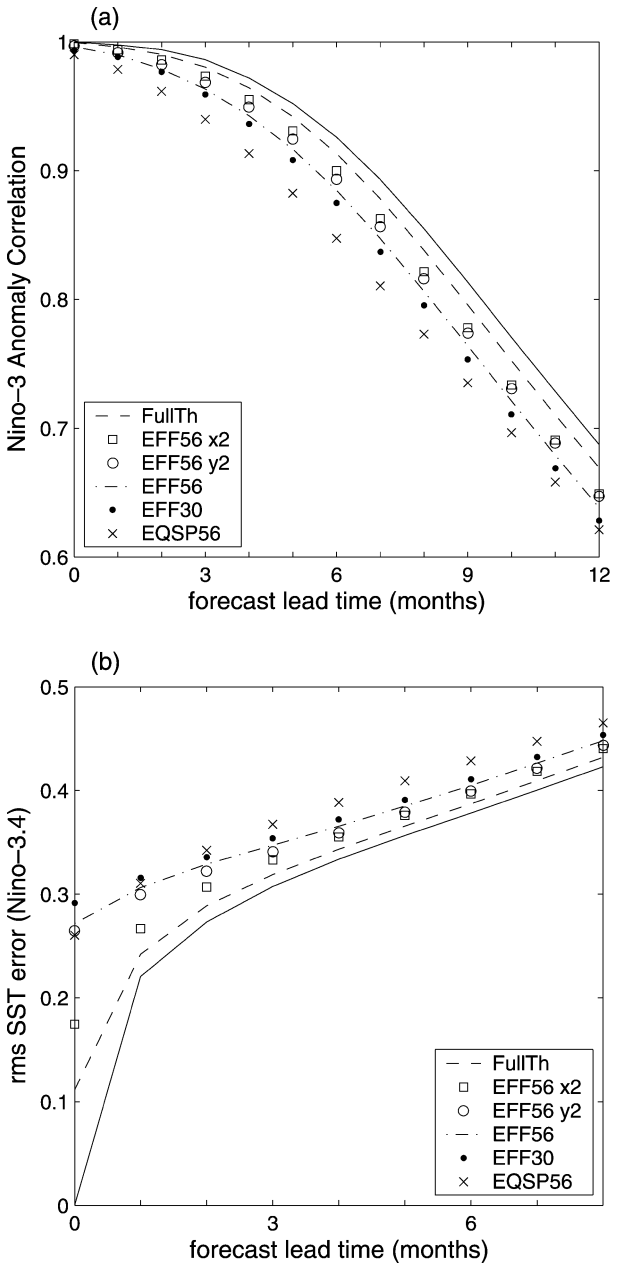

FIG. 4. (a) As in Fig. 2, but for the observing networks described in Table 2. The EFF30 and EFF56 networks, depicted in Fig. 3, represent efficient allocations of observations when SST and thermocline depth data are taken at the same locations (on average, in this system). Note that the EFF56 and EFF56x2 results are the same as the 8x Alt−170W+114W and 15x results, respectively, in Fig. 2. (b) As in (a), but for rms SST error in the Niño-3.4 region, for forecast lead times up to 8 months. The solid line in both (a) and (b) depicts results from the PerfectIC experiment.

TABLE 2. Description of the observing networks for the results discussed in section 3a.

Network	Description
EFF56	Efficient network of 56 SST and thermocline depth observing locations, depicted in Fig. 3 (small dots).
EFF30	Efficient network of 30 SST and thermocline depth observing locations, depicted in Fig. 3 (circles); subset of locations in EFF56.
EFF56x2	Variant of EFF56, with the longitudinal density of observations approximately doubled (at the same 7 latitudes as EFF56, but at all 15 longitudinal grid points, for a total of 105 observing locations).
EFF56y2	Variant of EFF56, with the latitudinal density of observations approximately doubled (at the same 8 longitudes as EFF56, but at 13 latitudes equally spaced from 9.2°S to 9.2°N, for a total of 104 observing locations).
EQSP56	Network with the same number of observations as EFF56, but with the 56 observing locations evenly distributed in latitude and longitude and symmetric about the equator (at every other grid point in longitude, at 7 latitudes equally spaced from 9.2°S to 9.2°N).

are shown for two norms, Niño-3 AC and rms SST error in the Niño-3.4 region; results for the other norms tested are similar. First, compare the EFF56 results with those from the EQSP56, EFF56x2, and EFF56y2 networks. When the 56 observing locations in EFF56 are distributed evenly throughout the domain, as in EQSP56, forecasts are significantly less skillful. This confirms that EFF56 is a relatively efficient way to allocate 56 observing locations. When the number of observations in EFF56 is nearly doubled, to the EFF56x2 or EFF56y2 networks, Niño-3 anomaly correlation forecast skill increases by only a small amount. In the rms SST norms, the analyses produced by the EFF56x2 network have significantly smaller errors than EFF56 analyses, but these improved analyses have only a small effect on forecasts longer than 2 months. Together, these results demonstrate that EFF56 is a reasonably efficient observing network for forecasting ENSO in this system.

Next, compare the EFF30 results in Fig. 4 with those from the EFF56 and EQSP56 networks. At lead times of 9 months or shorter, EFF30 forecasts are nearly as skillful as EFF56 forecasts in all of the norms tested. And, at lead times of 3 months or longer, EFF30 forecasts are noticeably more skillful than EQSP56 forecasts. Because EFF30 has approximately half as many observations as EFF56, EFF30 is on average a more efficient observing network than EFF56 for forecasting ENSO 3–9 months in advance.

A comparison of the EFF56x2 and EFF56y2 results in Fig. 4 indicates that nearly doubling the number of longitudes with observations in EFF56 increases forecast skill more than nearly doubling the number of latitudes with observations. This suggests that if one were designing an efficient network to produce more skillful forecasts than EFF56, adding observations at unobserved longitudes in EFF56 would be more important than adding observations at unobserved latitudes. Additional experiments (results not shown) indicate that adding 7 observations along the equator (at the longi-

tudinal grid points that are unobserved in EFF56) produces approximately half of the Niño-3 AC forecast improvement between EFF56 and EFF56x2, and approximately one-third of the analysis and short-term forecast improvement in the rms SST norms. Achieving additional analysis and forecast improvements requires adding off-equatorial observations at additional longitudes. Given the small differences in forecast skill among these networks, however, and the assumptions in the experimental design, attributes of efficient SST- and thermocline-observing networks are not investigated in greater detail.

The effectiveness of the EFF56 and EFF30 networks suggests that forecasting ENSO skillfully might not require observations across the entire tropical Pacific. Instead, observations in a few well-chosen regions—the eastern Pacific between the equator and 9°S, and the western equatorial Pacific—might suffice. As discussed above, however, the observation voids in EFF56 and EFF30 do degrade analyses and short-term forecasts. Plots of the spatial distribution of time-averaged analysis and forecast errors (not shown) indicate that the analysis and short-term forecast degradations are concentrated in unobserved regions and propagate only slightly into longer-term forecasts. Because the longitudinal correlation length (1300 km) in the 3DVAR background error covariances is less than the longitudinal grid point spacing, the data assimilation system does not interpolate a large amount of observational information to unobserved longitudes; thus, with a more sophisticated data assimilation, such analysis degradations may be alleviated. In addition, Fig. 4a suggests that as the lead time increases, the observation voids in EFF30 and EFF56x2 have a greater influence on forecast skill. Given this information, the choice between an observing network with broad coverage and one with limited coverage would depend on a number of factors, including the forecast norm and lead time of greatest interest, the forecast skill desired, the available resources for observations, the data assimilation system, and the importance of observations or accurate domain-wide analyses for uses besides operational ENSO forecasting.

b. Efficient networks of thermocline depth observations, assuming many SST observations

Real-time SST information is currently available from a number of sources besides the TAO moorings, including satellites, drifting buoys, and ships. In fact, SST information is currently available with sufficient spatial and temporal resolution that global SST analyses are generated operationally each week on a 1° grid (Reynolds and Smith 1994). Consequently, although the SST data from the TAO array remain useful for calibrating data from other sources and for filling in data gaps, one can generally assume that monthly SST is well observed. This section, therefore, explores efficient networks of observations that observe thermocline depth only, assuming that good SST information is already available from another source. For simplicity, when simulating this SST information, we do not account for the errors likely in a satellite- or analysis-based SST product; instead, we assume that the same type of SST observations as simulated earlier (uncorrelated errors, standard deviation of observation error = 0.2°C) are available each month at the 375 locations shown in Fig. 1.

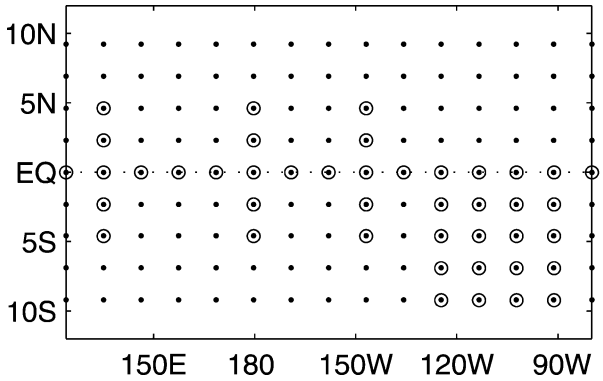

FIG. 5. Locations of the 43 thermocline depth observations in the EFFh43 network (circles) and the 135 thermocline depth observations in the EQSPh135 network (small dots), described in Table 3. Both networks have SST observations at the 375 locations shown in Fig. 1.

Note that satellites provide observations not only of SST, but also of sea level. As noted in section 2b, within the context of this model, assimilating thermocline depth information is similar to assimilating sea level or other upper-ocean heat content information. Thus, the results in this section can be interpreted as identifying important regions (in this system) for accurate heat content observations of any type, from in situ or remote sensing platforms.

To design efficient thermocline-observing networks when many SST observations are available, we performed experiments similar to those discussed in MB1 and section 3a, but moved only thermocline-observing locations. As discussed in MB1, when this simulated system has many reasonably accurate SST observations (FullT experiment), adding many thermocline depth observations (FullTh experiment) increases average forecast skill by only a small amount. Forecast skill for each of the networks tested for this section falls between that for FullT and FullTh. Consequently, the differences in forecast skill among the networks tend to be small. Although the small differences complicate identifying regions where thermocline depth observations are important, the results from many experiments were combined to design a sample efficient thermocline-observing network when many SST observations are available. This network, called EFFh43, has 43 observations at the locations indicated by the circles in Fig. 5.

Figure 6 shows the average skill of forecasts from the EFFh43, FullTh, and FullT networks, and from the EQSPh40, EQSPh45, and EQSPh135 networks described in Table 3. Results are shown for two norms,

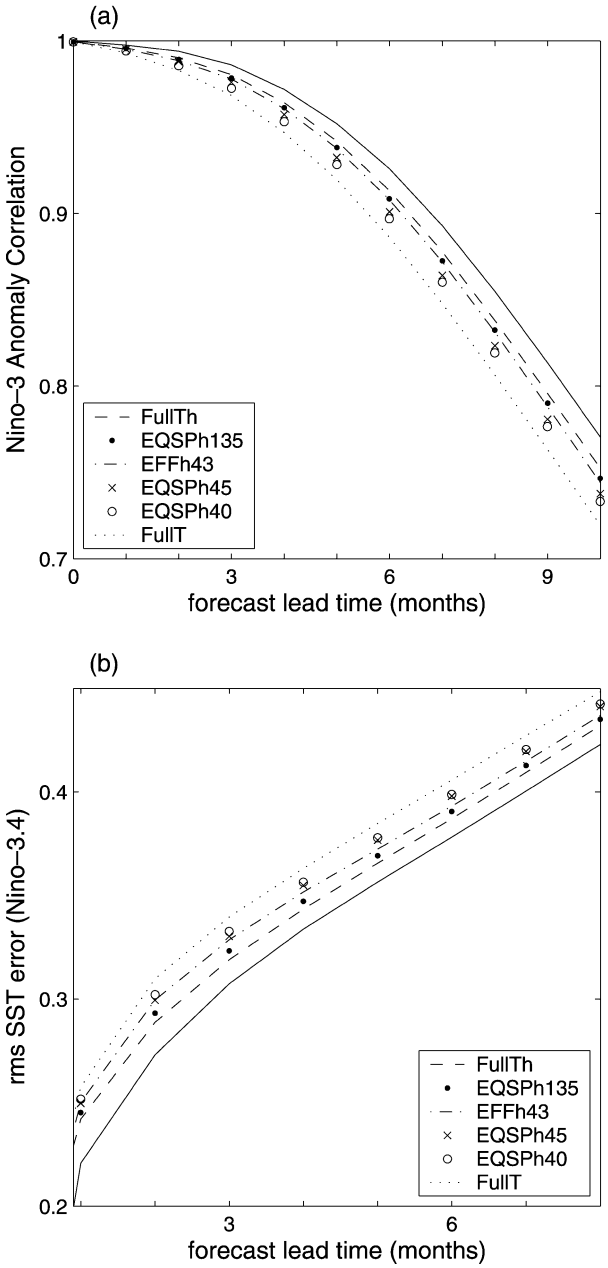

FIG. 6. (a) As in Fig. 2, but for the observing networks described in Table 3 and the FullT network described in Table 1, for forecast lead times up to 10 months. The EFFh43 network, shown in Fig. 5, represents an efficient allocation of thermocline depth observations (on average, in this system), assuming that many SST observations are available from another source. (b) As in (a), but for rms SST error in the Niño-3.4 region, for forecast lead times of 1–8 months. Results for analyses (0-month lead time forecasts) are identical for all networks. The solid line in both (a) and (b) depicts results from the PerfectIC experiment.

TABLE 3. Description of the observing networks for the results discussed in section 3b. All assume that SST observations are available at the 375 locations shown in Fig. 1.

Network	Description
EFFh43	Efficient network of 43 thermocline depth observations, depicted in Fig. 5 (circles).
EQSPh45	Network with approximately the same number of thermocline depth observations as EFFh43, but with the 45 locations evenly distributed in latitude and longitude and symmetric about the equator (at every grid point in longitude, at 4.6°S, 0°, and 4.6°N).
EQSPh40	Network with approximately the same number of thermocline depth observations as EFFh43, but with the 40 locations evenly distributed in latitude and longitude and symmetric about the equator (at every other grid point in longitude, at 9.2°S, 4.6°S, 0°, 4.6°N, and 9.2°N).
EQSPh135	Network with 135 thermocline-observing locations evenly distributed in latitude and longitude and symmetric about the equator, shown in Fig. 5 (small dots); includes all locations in EFFh43, EQSPh45, and EQSPh40.

Niño-3 SST AC and rms SST error in the Niño-3.4 region; results for the other norms tested are similar. Given the small difference between FullT and FullTh forecast skill, 4–10-month forecasts from EFFh43 are noticeably more skillful than those from EQSPh40 and EQSPh45, each of which has approximately the same number of thermocline observations as EFFh43 but has them distributed evenly throughout the domain. In addition, EFFh43 forecasts are only slightly less skillful than those from EQSPh135, a network with more than three times as many thermocline observations. When observations are removed from EFFh43 in different regions (results not shown), average forecast skill decreases. Together, these results confirm that EFFh43 is a relatively efficient configuration of thermocline depth observations for forecasting ENSO in this system.

EFFh43 is only a sample efficient observing network; for some forecast lead times and norms, other networks with approximately the same number of thermocline depth observations as EFFh43 can produce forecasts of similar skill. Although the locations of thermocline depth observations varies somewhat among these different efficient observing networks, they all have several features in common with EFFh43: an emphasis on observations in the southeastern equatorial Pacific from approximately 130° to 90°W and 0° to 9.2°S, observations along the equator across much of the Pacific, and several off-equatorial observations in the western Pacific at approximately 135°E. The off-equatorial observations in the central Pacific in EFFh43, near the date line and 150°W, are of lesser importance; they primarily improve analyses and short-term forecasts in the rms SST norms.

Note that, as discussed in section 3a, the correlation length in the data assimilation system background error covariance matrix is only 1300 km (less than the longitudinal gridpoint spacing) for both SST and ocean dynamics. Consequently, the data assimilation system does not interpolate much thermocline depth information from observed to unobserved grid points. With a

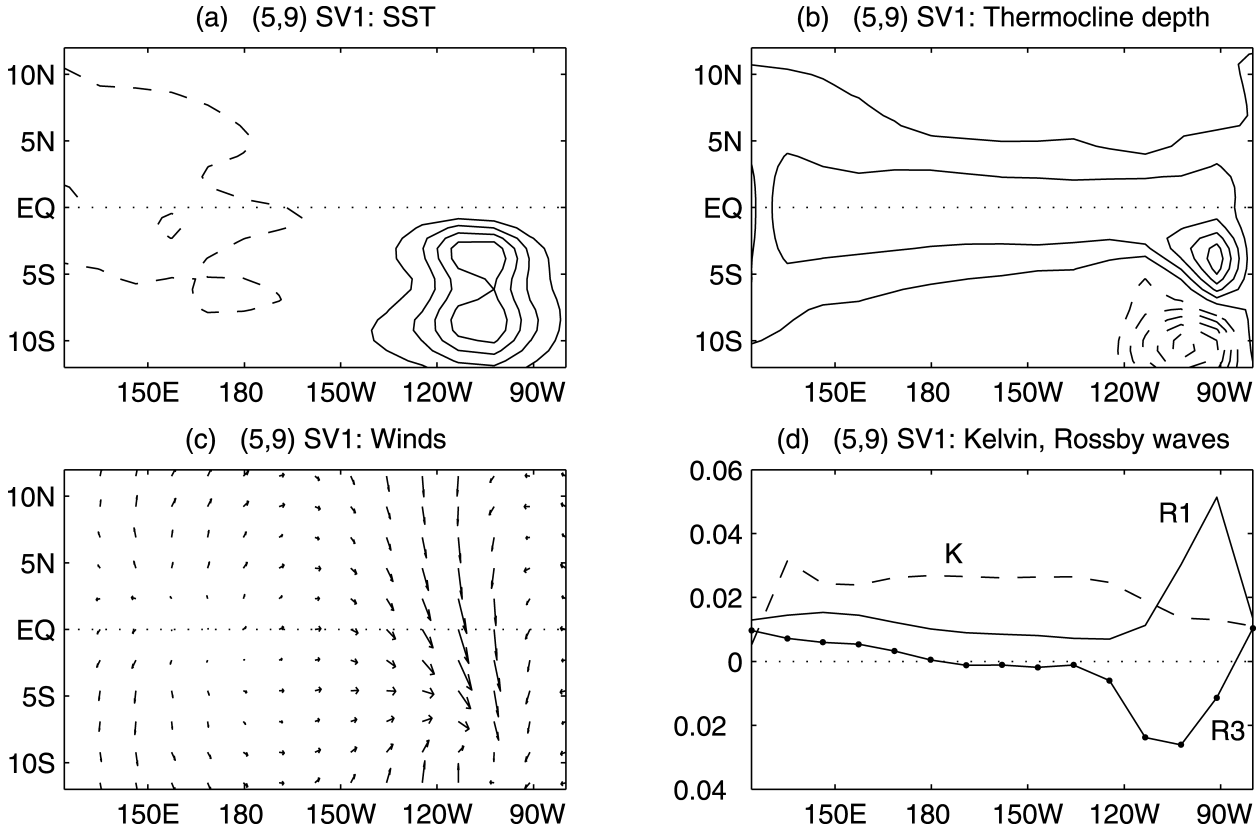

FIG. 7. Leading singular vector (optimal perturbation) for a 1 May start date and a 9-month optimization period (5,9), calculated as described in Thompson and Battisti (2000). The fields depicted are (a) SST, (b) thermocline depth, (c) atmospheric surface winds induced by (a), and (d) amplitude of the Kelvin wave (K, dashed) and the first two symmetric Rossby waves (R1, solid; R3, line with dots). The contour intervals are 0.2°C in (a) and 1 m in (b); the maximum wind vector in (c) is 0.22 m s^{-1}. The singular vector is scaled so that the absolute value of the SST field has a maximum of 1°C. The sign of the singular vector is such that it leads to an El Niño event; positive contours are solid and negative contours dashed. As discussed in Thompson (1998), a 1-2-1 zonal filter is applied.

more sophisticated data assimilation system, therefore, a network with fewer thermocline depth observations than EFFh43 might produce equally skillful forecasts.

c. Discussion

As discussed in MB1, error growth in this ENSO model is dominated by the leading singular vector (optimal perturbation). The leading singular vector has similar spatial structure for all start times for optimization times between 4 and 12 months, and it grows into the ENSO mode (Thompson and Battisti 2000). The leading singular vector therefore indicates which errors in initial conditions, if they exist, will grow most rapidly into errors in ENSO forecasts.

Singular vectors are calculated using the model's adjoint. The model's adjoint can also be used to calculate the sensitivity of a specified forecast norm (e.g., Niño-3 SST) to all perturbations in initial conditions. Because adjoint-derived sensitivities identify regions of sensitivity rather than a rapidly growing structure, interpreting their implications for observing system design can be more straightforward. As discussed in MB1, however, in this model, adjoint-derived sensitivities and leading singular vectors have similar spatial patterns for forecast (optimization) times longer than several months. Because only general features of the sensitivities/singular vectors are addressed, and because the ENSO literature depicts singular vectors more often than adjoint-derived sensitivities, in this paper we will illustrate regions of sensitivity to initial perturbations using singular vectors, with the understanding that adjoint-derived sensitivities identify similar regions.

Figures 7a–b depict the initial SST and thermocline depth fields of the leading singular vector for a 9-month optimization time starting in May, a local maximum in transient growth. Comparing Fig. 3 with Figs. 7a–b, one can see that the EFF56 and EFF30 networks, which observe SST and thermocline depth at the same locations, have observations where the singular vector has a large amplitude in SST and, to a lesser extent, in thermocline depth. The EFFh43 network shown in Fig. 5, which assumes that SST is already well observed, has thermocline observations where the singular vector has large amplitude in thermocline depth. In other words, efficient observing networks in this system gen-

erally take data in regions where the model's leading singular vector indicates that errors in initial conditions, if they exist, can grow most rapidly into errors in ENSO forecasts.

The correspondence between important regions for observations and the leading singular vector suggests that the physics behind the efficient observing networks can be understood in terms of the singular vector's dynamics (which are only summarized here; for further details, see Thompson 1998 and Thompson and Battisti 2000). As discussed by Chen et al. (1997), the singular vector has an SST maximum in the southeast equatorial Pacific (Fig. 7a) because this forces a northwesterly wind anomaly in the eastern equatorial Pacific (Fig. 7c). This relaxes the mean southeasterly wind stress in this region, decreasing the upwelling of cold water, which warms the eastern near-equatorial Pacific. The maximum is off of the equator because the thermal damping in the model peaks along the equator; it is slightly south rather than north of the equator because this is where upwelling is largest (Thompson 1998). The depressed thermocline in the southeast equatorial Pacific (Fig. 7b) also contributes to heating by increasing the temperature of upwelled water (Thompson 1998). Thus, information from the observations in the southeastern equatorial Pacific is communicated to the Niño-3 region primarily through upwelling.

As depicted in Fig. 7d, the singular vector has a positive Kelvin wave signal all along the equator, and a secondary positive Rossby wave signal in the western Pacific. As these Kelvin waves propagate to the eastern Pacific, they depress the thermocline, enhancing the eastern equatorial Pacific SST anomaly; these Rossby waves have the same effect once they are reflected as Kelvin waves at the western boundary. Thus, information from observations in the western Pacific is communicated to the Niño-3 region primarily through ocean wave propagation. Because of the importance of these waves, all of the efficient observing networks have several observations in the equatorial western Pacific. In fact, the EFFh43 network has thermocline depth observations all along the equator, observing the equatorially trapped Kelvin waves as they are initiated and propagate eastward. The EFFh43 network also has an off-equatorial ''ladder'' structure to resolve the two gravest symmetric Rossby waves, which, as discussed by Battisti (1988), will be important for the evolution of the system after being reflected at the western boundary.

The correspondence between important regions for observations and the adjoint-derived sensitive regions in this system also suggests that singular vectors or adjoint-derived sensitivities could be used to design efficient observing networks for ENSO prediction.[1] Using singular vectors and sensitivities to identify important regions for observations has been discussed extensively and tested for numerical weather prediction (e.g., Dabberdt et al. 1996; Snyder 1996; Palmer et al. 1998; Langland 1999; Langland et al. 1999). Unlike in weather prediction, however, most studies of singular vectors in ENSO prediction indicate that error growth is dominated by the leading singular vector. Many studies also find that the leading singular vector's structure does not vary significantly with the optimization time (within the range of primary interest for forecasting) or phase of the ENSO cycle (Xue et al. 1994; Penland and Sardeshmukh 1995; Moore and Kleeman 1996; Chen et al. 1997; Kleeman and Moore 1997; Xue et al. 1997a,b; Thompson 1998; Thompson and Battisti 2000). This suggests that the leading singular vector of the real ENSO system could be used to design a time-invariant observing network that would forecast ENSO effectively in a variety of situations.

Several studies of ENSO singular vectors have derived leading singular vectors that have a qualitatively similar spatial structure to that shown in Fig. 7. For example, using the nonlinear version of the Battisti (1988) intermediate coupled model and the closely related Zebiak–Cane model, Xue et al. (1994), Chen et al. (1997), and Xue et al. (1997a) found a leading SST singular vector with north–south and east–west asymmetry and maximum values in the southeast equatorial Pacific. A qualitatively similar large-scale SST structure was derived by Penland and Sardeshmukh (1995) using a Markov model. Penland and Sardeshmukh (1995) also found that when observed SST anomalies have a reasonably large projection onto their initial singular vector, observed SST anomalies 7 months later tend to resemble mature ENSO events (represented by their evolved singular vector); in addition, they note that warm SST anomalies in the southeastern equatorial Pacific appear in previous studies of precursors to some ENSO events.

Other studies derive leading ENSO singular vectors that are different—in some cases very different—from that shown in Fig. 7. The leading singular vectors calculated by Fan et al. (2000), for example, have SST maxima in the central-eastern Pacific, but along the equator. The leading singular vectors in Moore and Kleeman (1996, 2001) and Moore et al. (2003) have a substantially different spatial structure, with maximum amplitudes in the western Pacific. Note, however, that the intermediate coupled model used in Moore and Kleeman (1996, 2001) solves for SST anomalies only along the equator, then assumes that SST anomalies decay away from the equator with a Gaussian structure. Their coupled model cannot therefore produce an SST singular vector with an off-equatorial maximum, which, as noted above, is an important aspect of the singular vector for the model used here. Note also that the leading singular vector depicted in Fig. 7 does have Kelvin wave amplitude across the equatorial Pacific, consistent with

[1] This result is not unexpected, but could not have been assumed a priori because factors besides error growth, such as initial condition errors and the data assimilation system, affect where observations are most important for forecasts.

the theory that ENSO can be initiated by westerly wind bursts associated with intraseasonal variability (e.g., Lau 1985; Moore and Kleeman 1999). The central and western Pacific components of this model's singular vector contribute to ENSO growth, but they do not contribute as much as the southeastern component of the singular vector, largely because their growth is not sustained for more than a few months.

The differences among these studies of ENSO's leading singular vector indicate that further study is required before our results can be applied to the real ENSO-observing network. More specifically, the results generated here are only applicable to the real ENSO-system to the extent that the model dynamics, including the regions most sensitive to initial perturbations, apply to the real ENSO system.

Several of the studies of ENSO singular vectors mentioned above also note that the leading singular vector's structure can vary with the choice of norm. This raises another important aspect of observing network design: the definition of ''efficient.'' The results in sections 3a–b indicate that modifying the definition of efficient, for example, by modifying the forecast norm and lead time of interest, can affect which network forecasts ENSO most skillfully. In addition, the definition of efficient used here incorporates two constraints—maximizing forecast skill and minimizing the number of observations—that no single observing network satisfies. This means that without additional information, there is no unique solution for an efficient observing network, even for this idealized system. Developing an efficient observing network therefore not only requires calculating singular vectors, running OSSEs or other model-based experiments, or experimenting with real data, but also requires selecting an appropriate forecast norm and lead time, and then balancing the two components of efficient (benefits and costs) using information about the forecast skill desired, the costs of various observing platforms, and the resources available for observations.

4. Studying ENSO prediction with data records of limited duration

Although observations of the tropical Pacific have been collected for more than 100 years, only in the last several decades have enough observations been regularly available to construct reasonably complete pictures of tropical Pacific SST or surface wind stress on monthly or shorter time scales. The period of time with reasonably complete information about ocean heat content, for example, subsurface ocean or sea level observations, is even shorter. For this reason, most published studies of observing requirements for ENSO prediction that use real data examine fewer than 30 years of ENSO events (e.g., Chen et al. 1998; Johnson et al. 2000; Xue et al. 2000), and many of the frequently cited studies examine fewer than 15 years of events (e.g., Kleeman et al. 1995; Fischer et al. 1997; Ji and Leetmaa 1997; Rosati et al. 1997).

In contrast, when running OSSEs, the number of ENSO events that can be studied is limited only by the computer resources available to generate the synthetic data. All of the results shown in MB1 and section 3 are for runs of 1000 years, an order (or two) of magnitude longer than the real-world data record useable for similar experiments. To facilitate comparing the results presented here with those from studies with real data, this section briefly examines the sensitivity of the OSSE results to the duration of the simulated data record.

The results for this section were generated by rerunning OSSEs discussed earlier for a longer period of time (e.g., 100 000 yr). Each run was partitioned into shorter time segments of equal length (e.g., a hundred 1000-yr segments), and the average analysis and forecast skill was calculated independently for each time segment. This procedure was then repeated for different segment lengths (e.g., a thousand 100-yr segments) to simulate data records of different lengths. The results are examined in two ways. First, to evaluate how the available data record can affect estimates of ENSO predictability, we compare results averaged over different time segments within the same experiment. Second, to evaluate how the available data record can affect the relative skill of forecasts from different observing networks, we compare results from different experiments averaged over the same time segment.

a. Estimating the predictability of ENSO

Figure 8 depicts the variability in forecast skill when a 100 000-yr run of the PerfectIC experiment (described in Table 1) is divided into consecutive 1000-, 100-, and 30-yr segments. Recall that the PerfectIC results represent the maximum forecast skill attainable by improving the initial conditions, a measure of potential ENSO predictability. Figure 8 therefore indicates how likely predictability estimated from a 1000-, 100-, or 30-yr data sample is to be representative of the true potential predictability of the system.

To discuss the variability in predictability illustrated in Fig. 8, here we use the forecast lead time at which the average Niño-3 SST AC drops below 0.6. When 1000 yr of data are available (Fig. 8a), estimates of predictability depend somewhat on the 1000-yr period sampled, but not significantly; Niño-3 AC drops below 0.6 for lead times between 13 and 16 months. With 100 yr of data (Fig. 8b), the variability increases; the Niño-3 AC can be less than 0.6 at a 10-month lead time or remain above 0.6 for lead times greater than 24 months. With only 30 yr of data (Fig. 8c), the variability is dramatic; in some 30-yr periods, the average Niño-3 AC is less than 0.6 for 8-month forecasts, while in others, 24-month forecasts retain significant skill (AC of 0.75). Recall that there is no long-term variability imposed in the model; the forecast skill varies with the time segment

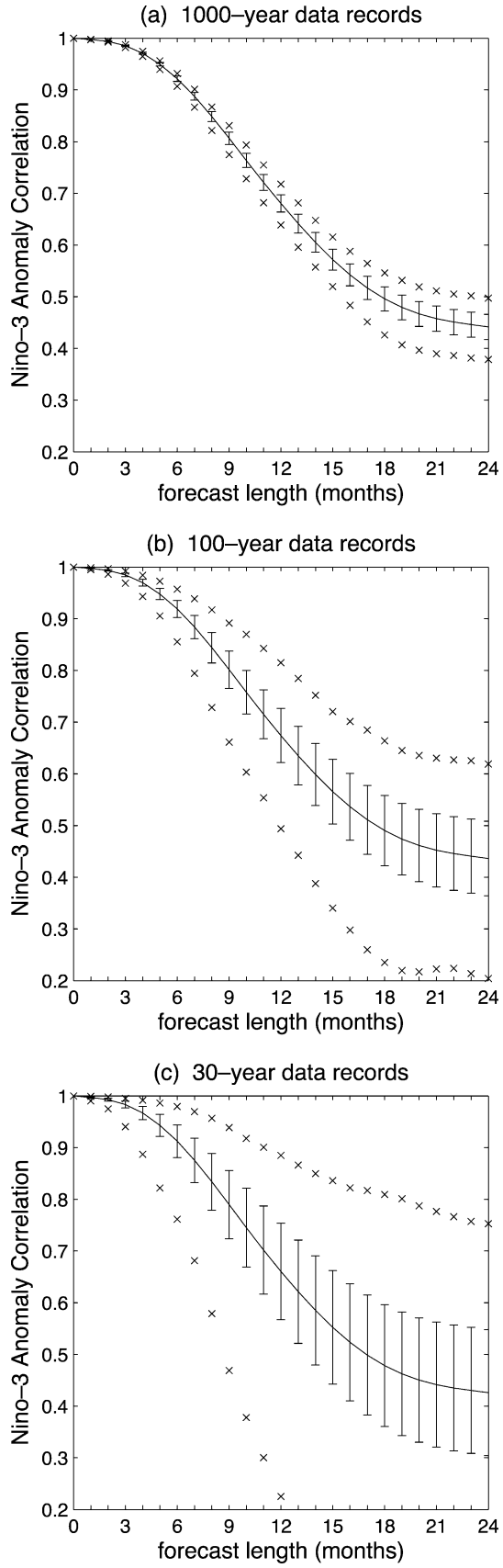

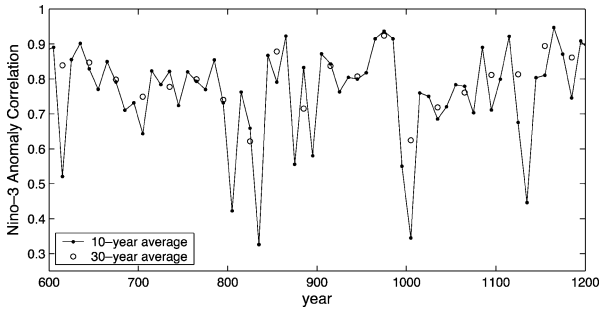

FIG. 9. Time series of the 9-month forecast skill from the PerfectIC experiment, averaged over consecutive 10- or 30-yr periods. Each small dot depicts the forecast skill averaged over a 10-yr period, plotted at the midpoint of the 10-yr period and connected by a solid line. Each circle depicts forecast skill averaged over a 30-yr period, plotted at the midpoint of the 30-yr period. Results are shown for an arbitrary 600-yr period taken from a longer OSSE.

only because the time segments contain different sequences of stochastic forcing, which excite different sequences of ENSO events. The apparent variability in ENSO predictability on time scales of decades or centuries is therefore due entirely to insufficient sampling of events. As illustrated by the time series of 10- and 30-yr average results in Fig. 9, the skill of forecasts from perfect initial conditions often does not shift gradually from one time segment to the next—this system can undergo rapid shifts in apparent predictability on time scales of one or several decades.

The ability of stochastic forcing, on its own, to generate the appearance of decadal and longer ENSO predictability ''regimes'' has been demonstrated previously by Kirtman and Schopf (1998) and Flügel and Chang (1999; see also Thompson and Battisti 2001). As discussed in Flügel and Chang (1999) and Thompson and Battisti (2001), stochastic forcing is also capable of inducing shifts in seasonality characteristics of ENSO predictability similar to those that have been observed in the real ENSO system within the last few decades. These results suggest that, even with a perfect model, it may be difficult to estimate the true potential predictability of ENSO using decades or even centuries of data. A more important issue for this paper is how this variability in ENSO predictability affects ENSO-observing network design; this is addressed next.

←

FIG. 8. (a) As in Fig. 2 for the PerfectIC experiment, but with results calculated separately for each of the 100 consecutive 1000-yr segments in a 100 000-yr OSSE (after spinup) for forecast lead times up to 24 months. At each lead time, the solid line depicts the mean of the ACs from the 100 time segments, the error bars depict the standard deviations of the ACs, and the crosses depict the maximum and minimum ACs. (b) As in (a), for the same 100 000-yr OSSE divided into one thousand 100-yr segments. (c) As in (a), for the same 100 000-year OSSE divided into 3333 30-yr segments. When the results in (b) and (c) are depicted for only 100 segments [the same number depicted in (a)], the variability is not substantially reduced from that shown.

b. Designing observing networks

As the predictability of ENSO varies with the time segment, the skill of forecasts produced by different observing networks tends to vary in a similar way. In other words, if the results in, for example, Fig. 2 are plotted for different 1000-, 100-, and 30-yr segments, forecast skill from the different experiments tends to move up and down together. Consequently, when comparing observing networks, the results do not depend on the duration of the simulated data record and the realization of that data record as much as Figs. 8–9 might suggest.

To illustrate this, Fig. 10 compares the skill of 6-month forecasts from the EFF56 and EQSP56 networks, averaged over each of the consecutive 100-, 30-, and 10-yr segments in a 10 000-yr run. The OSSEs for the two networks are run with the same sequence of stochastic forcing, that is, the same sequence of true states; each small dot in Fig. 10a (10b, 10c) therefore compares the ability of the EFF56 and EQSP56 networks to forecast the same 100-yr (30-yr, 10-yr) sequence of ENSO events. Recall from Fig. 4 that when statistics are accumulated over 1000 yr of data, 6-month forecasts from EFF56 are clearly more skillful than those from EQSP56.

When results are averaged over 100 yr of data (Fig. 10a), the relative skill of EFF56 and EQSP56 forecasts is similar for all time segments. When results are averaged over 30 yr of data (Fig. 10b), the magnitude of the difference between the EFF56 and EQSP56 results depends on the data sample, but the sign of the difference generally does not. When only 10 yr of data are available (Fig. 10c), EFF56 is more effective than EQSP56 for approximately 90% of the data samples. Given the large variability in predictability over 10- and 30-yr periods that is evident in Figs. 8–9, it is notable that sampling only 30 yr of ENSO events is sufficient to determine that the EFF56 network on average forecasts ENSO more skillfully than the EQSP56 network. These results suggest that even though short data records may make it difficult to ascertain the long-term (true) potential predictability of ENSO, they may still be useful for evaluating ENSO-observing networks.

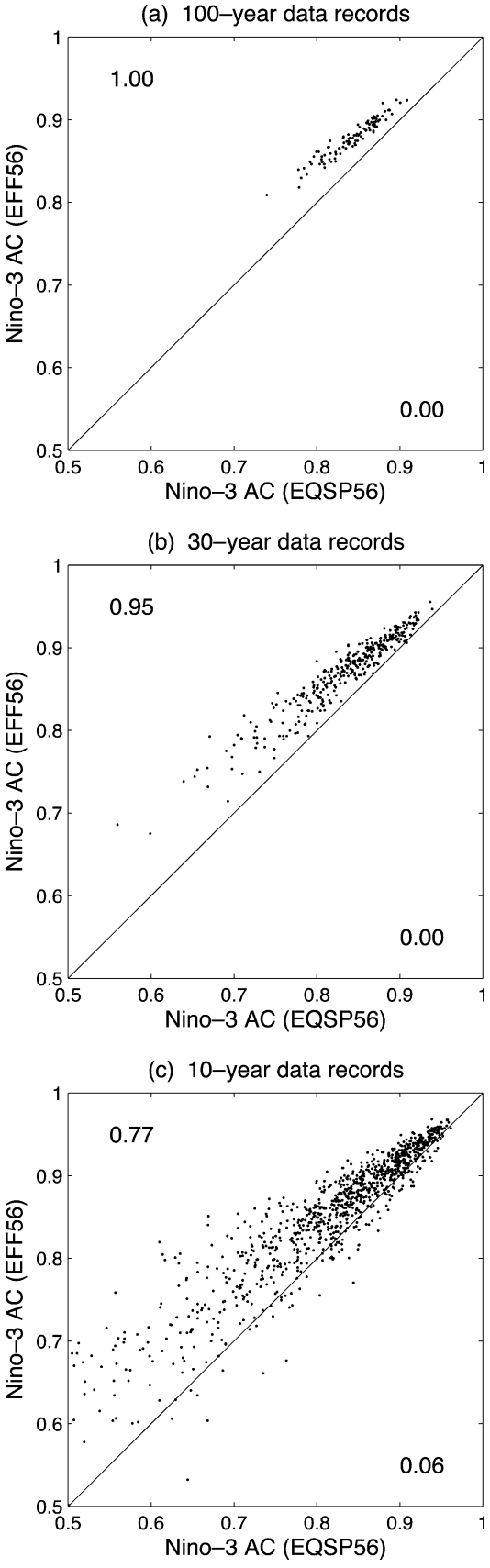

→

FIG. 10. (a) Skill (average Niño-3 AC) of 6-month forecasts from the EFF56 observing network plotted vs skill of 6-month forecasts from the EQSP56 observing network, for each of the 100 consecutive 100-yr segments in a 10 000-yr OSSE (after spinup). The networks are described in Table 2. Each small dot above the line indicates a 100-yr segment during which the 6-month forecasts from the EFF56 network are on average more skillful than those from the EQSP56 network; each small dot below the line indicates a segment when the EFF56 forecasts are on average less skillful than the EQSP56 forecasts. The number in the upper left (lower right) corner is the fraction of time segments for which the EFF56 forecasts are more (less) skillful than the EQSP56 forecasts and for which $|AC_{EFF56} - AC_{EQSP56}| \geq 0.01$. (b) As in (a), but for 333 30-yr segments. (c) As in (a), but for 1000 10-yr segments.

5. Summary and discussion

In this study, observing network design for ENSO prediction is investigated with observing system simulation experiments (OSSEs) run using a stochastically forced, linearized intermediate coupled ENSO model and a three-dimensional variational data assimilation system. The OSSEs allow forecast skill to be compared for a large number of simulated ENSO events and configurations of observations, many more than can be tested using real data. The OSSE results are used to develop observing networks that are on average efficient for predicting ENSO in this system, where efficient is defined as producing reasonably skillful forecasts for relatively few observations. Two types of observing networks are considered: networks in which SST and thermocline depth data are taken at the same locations, and networks of only thermocline depth observations when SST is already well observed. In the context of this system, observing SST is similar to observing atmospheric surface winds, and observing thermocline depth is similar to observing sea level or upper-ocean heat content.

Consistent with the results from the first part of this study (MB1), efficient observing networks in this system take data in only a few regions of the domain. Because the data assimilation determines how the observations are incorporated into the model, the efficiency of various observing networks is highly dependent on the data assimilation system. However, to facilitate separating the effects of modifying the observing network from the effects of the data assimilation, this study uses an assimilation scheme with simple, time- and longitude-invariant error covariances. Thus, with a more sophisticated data assimilation system, networks with even fewer observations than those depicted here are likely to forecast ENSO equally or more effectively.

The configurations of the efficient observing networks indicate that, when SST and thermocline depth are observed at the same locations, the most important regions for observations in this system are 1) from 10°S to 0° between 150°W and the eastern boundary and 2) from 5°S to 5°N near 145°E. Within these regions, a meridional observational spacing of approximately 2.5° is sufficient to produce forecasts with close to the maximum achievable forecast skill. Note that in the first region, SST information is often unavailable from satellites due to cloud cover. This suggests that a regular source of in situ SST observations may be particularly important in the southeastern equatorial Pacific.

As discussed in the companion paper (MB1), nearly all of the ENSO forecast skill possible in this system can be achieved by observing and assimilating SST only. Consequently, when SST is well observed in this system, differences in forecast skill among different thermocline-observing networks are generally small. Nevertheless, the efficient thermocline-observing networks developed indicate that when good information about SST is available from another source (e.g., satellites), the most important regions for ocean heat content observations in this system are 1) from 10°S to 0° between 130° and 90°W, 2) along the equator, and 3) from 5°S to 5°N near 135°E. Such observations may be taken from in situ platforms, satellites, or a combination of platforms that together provide the required spatial and temporal coverage and accuracy.

These important regions for observations correspond to where this model's leading singular vector (optimal perturbation) and adjoint-derived sensitivities have a large amplitude, that is, regions where errors in initial conditions can grow rapidly into errors in ENSO forecasts. Based on the dynamics of the leading singular vector, information from the observations in the southeastern equatorial Pacific is communicated to the Niño-3 region primarily through upwelling. Information from the observations in the western equatorial Pacific is communicated to the Niño-3 region primarily through ocean wave propagation. Information from the central Pacific does affect forecasts slightly through the same mechanisms, but for forecasts longer than a few months, its effects are swamped by those of information from the southeastern and western equatorial Pacific.

Most studies of ENSO singular vectors agree that error growth is dominated by the leading singular vector, with a spatial structure that does not vary significantly with the forecast start or lead time (for the forecast lead times of primary interest). Together with the results presented here, this suggests that singular vectors may be a useful tool for designing networks of fixed location observations that can forecast ENSO effectively in a variety of situations. There is not, however, a consensus on the leading ENSO singular vector's spatial structure. Consequently, the real-world effectiveness of the observing networks developed here depends on how similar this model's leading singular vectors are to those of the real ENSO system.

The relative importance of ocean observations in different regions of the tropical Pacific has been investigated previously. Of the studies of ENSO prediction, two determined, similar to our results, that ocean initialization is more important in the eastern tropical Pacific than in the western or central tropical Pacific: Philander et al. (1987), who studied the equilibration of a tropical Pacific ocean general circulation model to surface wind forcing, and Sun et al. (2002), who performed identical twin experiments similar to those in this study, with a more sophisticated (extended Kalman filter) data assimilation but a simpler (one-dimensional) model. In contrast, Hao and Ghil (1994), assimilating simulated data to correct initial and systematic wind stress errors in a shallow water model, found that ocean observations were generally more important in the western equatorial Pacific. Given these studies' different experimental designs and the few aspects of ENSO-observing networks they investigated, however, it is difficult to compare their results with ours in greater detail. Although the relative importance of ocean observations in different

regions has also been examined in studies of tropical Pacific data assimilation (e.g., Miller 1990; Sheinbaum and Anderson 1990a,b; Carton et al. 1996), these studies focus on state estimation rather than prediction. Because accurate analyses and skillful forecasts may require different observations (see, e.g., section 3), results from such studies cannot be directly interpreted in terms of implications for ENSO prediction.

A major difference between this study and many other studies of ENSO prediction is the number of ENSO events examined. Consequently, we also investigated the dependence of the OSSE results on the duration of the simulated data record and on the sequence of ENSO events within the record. With stochastic forcing as the only mechanism that can generate long-term variability, this system passes through decadal and longer periods in which forecasts generated from perfect initial conditions have very different levels of skill (see also Kirtman and Schopf 1998; Flügel and Chang 1999). In other words, this system exhibits significant temporal variability in potential predictability. Comparisons of the skill of forecasts from different observing networks, however, exhibit significantly less temporal variability. This suggests that data records of one or several decades may not be a major limitation for designing observing networks for ENSO prediction.

Another result from this study is that the placement of observations in an efficient network depends on the forecast norm and lead time of interest, particularly for forecasts of several months or less. Furthermore, the definition of efficient used here incorporates two constraints, maximum forecast skill and a minimum number of observations, that cannot be satisfied simultaneously. This suggests that developing and applying an appropriate definition of efficient is an important component of ENSO-observing network design. Aspects of this definition to consider include the desired benefits of the observing network, the costs of various observing platforms (including the incremental costs of existing platforms), and the available resources for observations. The desired benefits of the observing network can be defined from a scientific prediction perspective, for example, as a level of forecast skill in a specified norm at a given lead time, or from a societal perspective, based on the benefits society is expected to derive from different ENSO forecasts.

Although OSSEs are a useful complement to studies with real data, they have a major limitation: the results are only applicable to the real world to the extent that the simulated system is an adequate representation of the real system. The model used here to simulate the ENSO system is well documented (Thompson 1998; Thompson and Battisti 2000, 2001) and is closely related to the Zebiak–Cane (1987) model, which has been used extensively in previous studies and has demonstrated predictive skill at lead times of several seasons (e.g., Latif et al. 1998). Nevertheless, the model is still a simplified representation of full coupled atmosphere–ocean dynamics and thus may not simulate all forms of ENSO evolution. Moreover, the observations tested (particularly those of thermocline depth) are idealized. Consequently, the results derived here cannot be applied directly to the real ENSO-observing system. Rather, the results illustrate the potential for OSSEs to contribute to ENSO-observing network design, and they identify several potentially important considerations for ENSO-observing networks for further study. Possible next steps include incorporating real data into the model predictions, performing OSSEs with ENSO models that contain different dynamics, or running OSSEs using a more complex numerical model to simulate the real ENSO system.

Acknowledgments. This research was partially funded by a grant to DSB from the NOAA Climate Observation Program. Much of the research was conducted while REM was supported by an Advanced Study Program postdoctoral fellowship at the National Center for Atmospheric Research.

REFERENCES

Balmaseda, M. A., M. K. Davey, and D. L. T. Anderson, 1995: Decadal and seasonal dependence of ENSO prediction skill. *J. Climate,* **8,** 2705–2715.

Battisti, D. S., 1988: Dynamics and thermodynamics of a warming event in a coupled tropical atmosphere–ocean model. *J. Atmos. Sci.,* **45,** 2889–2919.

Carton, J. A., B. S. Giese, X. Cao, and L. Miller, 1996: Impact of altimeter, thermistor, and expendable bathythermograph data on retrospective analyses of the tropical Pacific Ocean. *J. Geophys. Res.,* **101,** 14 147–14 160.

Chen, D., S. E. Zebiak, A. J. Busalacchi, and M. A. Cane, 1995: An improved procedure for El Niño forecasting: Implications for predictability. *Science,* **269,** 1699–1702.

——, M. A. Cane, S. E. Zebiak, and A. Kaplan, 1998: The impact of sea level data assimilation on the Lamont model prediction of the 1997/98 El Niño. *Geophys. Res. Lett.,* **25,** 2837–2840.

Chen, Y., D. S. Battisti, T. N. Palmer, J. Barsugli, and E. S. Sarachik, 1997: A study of the predictability of tropical Pacific SST in a coupled atmosphere–ocean model using singular vector analysis: The role of the annual cycle and ENSO cycle. *Mon. Wea. Rev.,* **125,** 831–845.

Dabberdt, W. F., T. W. Schlatter, and the Second Prospectus Development Team, 1996: Research opportunities from emerging atmospheric observing and modeling capabilities. *Bull. Amer. Meteor. Soc.,* **77,** 305–323.

Derber, J., and A. Rosati, 1989: Global oceanic data assimilation system. *J. Phys. Oceanogr.,* **19,** 1333–1348.

Fan, Y., M. R. Allen, D. L. T. Anderson, and M. A. Balmaseda, 2000: How predictability depends on the nature of uncertainty in initial conditions in a coupled model of ENSO. *J. Climate,* **13,** 3298–3313.

Federov, A. V., and S. G. Philander, 2000: Is El Niño changing? *Science,* **288,** 1997–2002.

Fischer, M., M. Latif, M. Flügel, and M. Ji, 1997: The impact of data assimilation on ENSO simulations and predictions. *Mon. Wea. Rev.,* **125,** 819–829.

Flügel, M., and P. Chang, 1999: Stochastically induced climate shift of El Niño–Southern Oscillation. *Geophys. Res. Lett.,* **26,** 2473–2476.

Gill, A. E., 1980: Some simple solutions for heat-induced tropical circulation. *Quart. J. Roy. Meteor. Soc.,* **106,** 447–462.

Hao, Z., and M. Ghil, 1994: Data assimilation in a simple tropical ocean model with wind stress errors. *J. Phys. Oceanogr.,* **24,** 2111–2128.

Hayes, S. P., L. J. Mangum, J. Picaut, A. Sumi, and K. Takeuchi, 1991: TOGA-TAO: A moored array for real-time measurements in the tropical Pacific Ocean. *Bull. Amer. Meteor. Soc.,* **72,** 339–347.

Ji, M., and A. Leetmaa, 1997: Impact of data assimilation on ocean initialization and El Niño prediction. *Mon. Wea. Rev.,* **125,** 742–753.

——, ——, and J. Derber, 1995: An ocean analysis system for seasonal to interannual climate studies. *Mon. Wea. Rev.,* **123,** 460–481.

——, ——, and V. E. Kousky, 1996: Coupled model predictions of ENSO during the 1980s and the 1990s at the National Centers for Environmental Prediction. *J. Climate,* **9,** 3105–3120.

Johnson, S. D., D. S. Battisti, and E. S. Sarachik, 2000: Empirically derived Markov models and prediction of tropical Pacific sea surface temperature anomalies. *J. Climate,* **13,** 3–17.

Kirtman, B. P., and P. S. Schopf, 1998: Decadal variability in ENSO predictability and prediction. *J. Climate,* **11,** 2804–2822.

Kleeman, R., and A. M. Moore, 1997: A theory for the limitation of ENSO predictability due to stochastic atmospheric transients. *J. Atmos. Sci.,* **54,** 753–767.

——, ——, and N. R. Smith, 1995: Assimilation of subsurface thermal data into a simple ocean model for the initialization of an intermediate tropical coupled ocean–atmosphere forecast model. *Mon. Wea. Rev.,* **123,** 3103–3113.

Langland, R. H., 1999: Workshop on targeted observations for extratropical and tropical forecasting. *Bull. Amer. Meteor. Soc.,* **80,** 2331–2338.

——, and Coauthors, 1999: The North Pacific Experiment (NORPEX-98): Targeted observations for improved North American weather forecasts. *Bull. Amer. Meteor. Soc.,* **80,** 1363–1384.

Latif, M., and Coauthors, 1998: A review of the predictability and prediction of ENSO. *J. Geophys. Res.,* **103,** 14 375–14 393.

Lau, K.-M., 1985: Elements of a stochastic-dynamical theory of the long-term variability of the El Niño/Southern Oscillation. *J. Atmos. Sci.,* **42,** 1552–1558.

McPhaden, M. J., and Coauthors, 1998: The Tropical Ocean–Global Atmosphere observing system: A decade of progress. *J. Geophys. Res.,* **103,** 14 169–14 240.

Miller, R. N., 1990: Tropical data assimilation experiments with simulated data: The impact of the tropical ocean and global atmosphere thermal array for the ocean. *J. Geophys. Res.,* **95,** 11 461–11 482.

Moore, A. M., and R. Kleeman, 1996: The dynamics of error growth and predictability in a coupled model of ENSO. *Quart. J. Roy. Meteor. Soc.,* **122,** 1405–1446.

——, and ——, 1999: Stochastic forcing of ENSO by the intraseasonal oscillation. *J. Climate,* **12,** 1199–1220.

——, and ——, 2001: The differences between the optimal perturbations of coupled models of ENSO. *J. Climate,* **14,** 138–163.

——, J. Vialard, A. T. Weaver, D. L. T. Anderson, R. Kleeman, and J. R. Johnson, 2003: The role of air–sea interaction in controlling the optimal perturbations of low-frequency tropical coupled ocean–atmosphere modes. *J. Climate,* **16,** 951–968.

Morss, R. E., and D. S. Battisti, 2004: Evaluating observing requirements for ENSO prediction: Experiments with an intermediate coupled model. *J. Climate,* **17,** 3057–3073.

Palmer, T. N., R. Gelaro, J. Barkmeijer, and R. Buizza, 1998: Singular vectors, metrics, and adaptive observations. *J. Atmos. Sci.,* **55,** 633–653.

Penland, C., and P. D. Sardeshmukh, 1995: The optimal growth of tropical sea surface temperature anomalies. *J. Climate,* **8,** 1999–2024.

Perigaud, C. M., C. Cassou, B. Dewitte, L.-L. Fu, and J. D. Neelin, 2000: Using data and intermediate coupled models for seasonal-to-interannual forecasts. *Mon. Wea. Rev.,* **128,** 3025–3049.

Philander, S. G. H., W. J. Hurlin, and R. C. Pacanowski, 1987: Initial conditions for a general circulation model of tropical oceans. *J. Phys. Oceanogr.,* **17,** 147–157.

Reynolds, R. W., and T. M. Smith, 1994: Improved global sea surface temperature analyses using optimum interpolation. *J. Climate,* **7,** 929–948.

Rosati, A., K. Miyakoda, and R. Gudgel, 1997: The impact of ocean initial conditions on ENSO forecasting with a coupled model. *Mon. Wea. Rev.,* **125,** 754–772.

Sheinbaum, J., and D. L. T. Anderson, 1990a: Variational assimilation of XBT data. Part I. *J. Phys. Oceanogr.,* **20,** 672–688.

——, and ——, 1990b: Variational assimilation of XBT data. Part II: Sensitivity studies and use of smoothing constraints. *J. Phys. Oceanogr.,* **20,** 689–704.

Snyder, C., 1996: Summary of an informal workshop on adaptive observations and FASTEX. *Bull. Amer. Meteor. Soc.,* **77,** 953–961.

Sun, C., Z. Hao, M. Ghil, and J. D. Neelin, 2002: Data assimilation for a coupled ocean–atmosphere model. Part I: Sequential state estimation. *Mon. Wea. Rev.,* **130,** 1073–1099.

Thompson, C. J., 1998: Initial conditions for optimal growth in a coupled ocean–atmosphere model of ENSO. *J. Atmos. Sci.,* **55,** 537–557.

——, and D. S. Battisti, 2000: A linear stochastic dynamical model of ENSO. Part I: Model development. *J. Climate,* **13,** 2818–2832.

——, and ——, 2001: A linear stochastic dynamical model of ENSO. Part II: Analysis. *J. Climate,* **14,** 445–466.

Wallace, J. M., E. M. Rasmusson, T. P. Mitchell, V. E. Kousky, E. S. Sarachik, and H. von Storch, 1998: On the structure and evolution of ENSO-related climate variability in the tropical Pacific: Lessons from TOGA. *J. Geophys. Res.,* **103,** 14 241–14 259.

Xue, Y., M. A. Cane, S. E. Zebiak, and M. B. Blumenthal, 1994: On the prediction of ENSO: A study with a low-order Markov model. *Tellus,* **46A,** 512–528.

——, ——, and ——, 1997a: Predictability of a coupled model of ENSO using singular vector analysis. Part I: Optimal growth in seasonal background and ENSO cycles. *Mon. Wea. Rev.,* **125,** 2043–2056.

——, ——, ——, and T. N. Palmer, 1997b: Predictability of a coupled model of ENSO using singular vector analysis. Part II: Optimal growth and forecast skill. *Mon. Wea. Rev.,* **125,** 2057–2073.

——, A. Leetmaa, and M. Ji, 2000: ENSO prediction with Markov models: The impact of sea level. *J. Climate,* **13,** 849–871.

Zebiak, S. E., and M. A. Cane, 1987: A model El Niño–Southern Oscillation. *Mon. Wea. Rev.,* **115,** 2262–2278.